

## Silicon vacancy in SiC as a promising quantum system for single-defect and single-photon spectroscopy

Pavel G. Baranov,<sup>\*</sup> Anna P. Bundakova, and Alexandra A. Soltamova  
*Loffe Physical-Technical Institute, St. Petersburg, RU-194021 Russia*

Sergei B. Orlinskii  
*Federal Center of Shared Facilities of Kazan State University, RU-420008 Kazan, Russia*

Igor V. Borovykh,<sup>†</sup> Rob Zondervan, Rogier Verberk, and Jan Schmidt  
*Huygens Laboratory, Leiden University, P.O. Box 9504, 2300 RA Leiden, The Netherlands*  
(Received 29 August 2010; revised manuscript received 26 December 2010; published 14 March 2011)

Results of experiments are presented that suggest that the Si vacancy in SiC is a promising quantum system for single-defect and single-photon spectroscopy in the infrared region. The investigation was carried out with electron paramagnetic resonance (EPR), zero-field optically detected magnetic resonance (ODMR), direct-detection EPR (DD-EPR), and high-resolution fluorescence-excitation spectroscopy. Depending on the temperature, crystal polytype, and crystal position, two opposite schemes have been observed for the optical alignment of the populations of the spin sublevels of the high-spin ground state of the Si vacancy in SiC upon irradiation with unpolarized light at the zero-phonon lines (ZPLs). A giant change has been found in the luminescence intensity of the ZPLs in zero magnetic field upon the application of resonant microwaves which induce transitions between the spin sublevels of the vacancy ground state thus opening the possibility for magnetic-resonance detection of a single vacancy. The optical alignment of the populations of the spin sublevels in the ground state of the Si vacancy was shown with DD-EPR. Surprisingly narrow ZPLs of Si vacancies with a width less than 0.05 meV have been observed which seem to be the narrowest detected so far in SiC.

DOI: [10.1103/PhysRevB.83.125203](https://doi.org/10.1103/PhysRevB.83.125203)

PACS number(s): 61.72.jd, 61.72.Hh, 71.55.-i, 76.70.Hb

### I. INTRODUCTION

In recent years, single-molecule spectroscopy has been substantially developed<sup>1</sup> and magnetic resonance has been detected of single molecules<sup>1-4</sup> and single defects.<sup>5-8</sup> In connection with the development of quantum computers, the possibility of detecting and manipulating the spin states of a single localized electron in a solid is of special interest. The only known solid-state system where such manipulations have become possible<sup>5-8</sup> is the nitrogen-vacancy (NV) defect in diamond which represents a vacancy in the nearest environment of which a carbon atom is replaced by nitrogen. The optically detected magnetic resonance (ODMR) in a single NV defect at a microwave frequency of 2.87 GHz corresponding to the fine-structure splitting has become possible because of the existence of a unique cycle of optical alignment and the creation of an inverse population of triplet sublevels in the defect ground state. The duration of the spin alignment is restricted by spin-lattice relaxation caused by the effect of the nuclear magnetic moment of the substitutional nitrogen present in the diamond lattice.<sup>9,10</sup>

Owing to their unsurpassed photostability, defects in solids may be ideal candidates for single-photon sources.<sup>11</sup> In the context of a single-photon source for fiber optic communications, a serious disadvantage of the NV defect in diamond is its emission wavelength, which is around 640 nm. At this wavelength standard silica glass optical fibers exhibit an attenuation of about 7 dB/km whereas for wavelength of 800 nm it is 2.8 dB/km and strongly decreases with an increase in wavelength.

Thus, a search for systems possessing the unique properties of the NV defect in diamond but without its disadvantages such as the occurrence of nitrogen nuclear magnetic moments, a high-microwave frequency, and the invariability of its optical and microwave parameters is very promising.

A combination of photons with single defects could be an attractive scheme for quantum computing. The smallest area on which one can focus light contains many defects with spins (qubits). The limit of optical spatial resolution (about  $1 \mu\text{m}^3$ ) is a factor 100 larger than defect spacings needed for entanglement. To address chosen pairs of qubits one can exploit the randomness inevitable in standard fabrication and doping.<sup>12</sup> Light of different wavelengths will excite different control spins in a patch, and so manipulate the entanglements of different qubits. Recent investigations aimed to find new defects applicable and even more favorable for quantum computing than NV centers in diamond. Among them such centers nitrogen-vacancy defects<sup>13-15</sup> and silicon vacancy<sup>16</sup> in SiC were proposed. The latter are attractive because they exhibit a multitude of ZPLs in the region of 850–920 nm, which coincides with the spectral window of silica glass optical fiber. The host and defect criteria that have to be satisfied in order to design quantum qubits were postulated in Ref. 14.

The hexagonal 4H- and 6H-SiC polytypes are the most common and most appropriate for applications and have the band gap of 3.2 and 3.0 eV, respectively,<sup>17</sup> and a very small spin-orbit coupling. The isotopic engineering of the SiC crystals can be performed via the sublimation technique<sup>18-20</sup> which allows the reduction of the natural abundance of nuclear spins of <sup>29</sup>Si (4.7%) and <sup>13</sup>C (1.1%) and is technology that has

been available a long time. Vacancies are the primary defects in SiC and present at the various sites in the different polytypes that arise from differences in the stacking sequence of the Si and C layers. In 4H-SiC two nonequivalent crystallographic positions exist, one hexagonal and one quasicubic site, called  $h$  and  $k$ , respectively. In 6H-SiC three nonequivalent positions are formed, one hexagonal and two quasicubic ones, called  $h$ ,  $k1$ , and  $k2$ .

Two important experimental tools for the identification and study of the defects in semiconductors are (electron paramagnetic resonance) EPR and ODMR.<sup>21</sup> In this work, it is shown that silicon vacancies in silicon carbide can be considered as promising objects for single-defect spectroscopy. As distinct from the NV defect in diamond, two opposite cycles have been observed for the optical alignment of the spin sublevels in the ground state, a property that makes the Si vacancy in SiC in many respects superior to the NV center in diamond.

## II. EXPERIMENTAL

Crystals of the two main silicon carbide polytypes were studied: 4H-SiC and 6H-SiC. Si vacancies were introduced by irradiation with fast neutrons at room temperature with a dose of  $10^{15}$  cm<sup>-2</sup>– $10^{16}$  cm<sup>-2</sup> or by quenching the samples from a temperature of 2300 °C. One set of neutron-irradiated samples was labeled as sample no. 1 (6H-SiC, dose of  $10^{15}$  cm<sup>-2</sup>) and sample no. 2 (4H-SiC, dose of  $10^{16}$  cm<sup>-2</sup>). The second set of the samples was labeled as sample no. 3 (6H-SiC quenched from  $T = 2300$  °C), sample no. 3a (sample no. 3 annealed at 750 °C during 30 min), sample no. 3b (sample no. 3 annealed at 750 °C during 60 min), sample no. 3c (sample no. 3 annealed at 750 °C during 120 min).

The EPR spectra were detected at an X-band (9.3 GHz) on a continuous wave (cw) spectrometer in the temperature range 4–300 K. The samples, in the shape of platelets, had a dimension of about  $3 \times 4 \times 0.4$  mm<sup>3</sup>. The samples were oriented to allow rotation in the  $1\bar{1}\bar{2}0$  plane.

In the present work a direct-detection EPR (DD-EPR) technique was used.<sup>22,23</sup> Its high-time resolution (ca. 50 ns) allows detecting signals shortly after the exciting laser flash, before any significant relaxation between spin sublevels has taken place. DD-EPR experiments were performed as described earlier.<sup>22,23</sup> In short, a home-built X-band EPR spectrometer was used, equipped with a Varian rectangular TE102 optical transmission cavity. A laser pulse initiated a reaction producing paramagnetic states. Following the flash, a boxcar sampled the changes in microwave power reflected from the cavity. For obtaining transient EPR spectra, the sampling gate width of 1.3  $\mu$ s and its delay of 0.2  $\mu$ s after the flash were fixed, and the magnetic field was slowly swept while the output signal of the boxcar was recorded. In the DD-EPR experiment the signal appeared in direct absorption and emission mode. The overall time resolution of our setup was about 50 ns.

An Oxford Instruments helium gas-flow cryostat regulated the temperature with a home-built temperature controller, which could be set with 1 K accuracy, and stabilized the temperature to about 0.2 K. As an excitation light source, a Continuum Surelight I-pumped OPO laser was used with a flash duration of ca. 4 ns and an output power of about 3 mJ.

Samples were excited into the near-infrared absorption band with an excitation bandwidth of 4–5 nm.

The experiments with resonant optical excitation were carried out with a broad band (30 GHz) titanium-sapphire laser (Ti:Sa) with longitudinal cavity, model 3900S from Spectra-Physics, pumped by an argon-ion laser (Spectra-Physics Stabilite 2017) at multiline operation. Typical output powers were 160–400 mW. The single-mode excitation in high-resolution experiments was performed through a fiber with a Coherent 899-21 Ti:Sa ring laser with a bandwidth of 500 kHz equipped with an autoscan and pumped by a Coherent Innova 200 argon-ion laser. By this system output powers up to 100 mW could be produced with the highest energy density on the sample of 8 W/cm<sup>2</sup>. In the high-resolution experiments a monochromator was used instead of a band-pass filter to be sure to see only emission from the silicon vacancy and not from other defects. For detection two germanium detectors from Northcoast were used with a sensitivity range from 800 to 2000 nm. The radio-frequency (rf) fields applied in the ODMR experiments were produced by a HP synthesized sweeper and amplified up to 40 dBm (10 W) by an rf amplifier.

The confocal arrangement is nowadays the standard setup for single-defect microscopy/spectroscopy and described elsewhere.<sup>1</sup> The laser light is focused on the sample by the same objective that collects the fluorescence. The confocal arrangement reduces the excitation or detection volume to several cubic microns. This volume is typically 1–10  $\mu$ m<sup>3</sup>. A smaller excitation and detection volume causes less background.

## III. RESULTS AND ANALYSIS

### A. EPR

Figure 1 shows cw X-band (9.4 GHz) EPR spectra of vacancies detected at sample nos. 1 (a), 2 (b), and (c). Spectra were recorded without light (dashed line) and under continuous optical illumination with unfiltered light of a 100-W xenon lamp with the magnetic field parallel to the  $c$  axis ( $B \parallel c$ ). There are two dominant types of EPR spectra present in Figs. 1(a) and 1(b). The central signal, marked by  $V_{Si}^-$ , is accompanied by a set of hyperfine (HF) lines with a splitting of 0.29 mT and an intensity ratio to the central line of about 0.3. This spectrum is attributed to the negatively charged silicon vacancy  $V_{Si}^-$  with  $S = 3/2$  and a fine structure splitting  $D$  close to zero.<sup>25</sup> In quenched 6H-SiC (sample no. 3) strong EPR signal of the shallow  $N^0$  donors was observed [Fig. 1(c)].

Two more sets of EPR spectra in Fig. 1(a) indicated by  $V_{Si}(h)$  and  $V_{Si}(k1,k2)$  are attributed to the silicon vacancy. Here, symbols “ $h$ ” and “ $k1, k2$ ” indicate the hexagonal and the quasicubic positions in the 6H-SiC crystal that has a hexagonal symmetry with symmetry axis  $c$ . In Figs. 1(b) and 1(c) only the set belonging to  $V_{Si}(h)$  was observable in the EPR spectra. The assignment to these sites was made with the assumption that a defect at a hexagonal site experiences a stronger axial crystal field than a defect on a quasicubic site and that consequently the zero-field splitting for the hexagonal site is larger than that for the quasicubic site. The intensity of the inner doublet ( $k1, k2$  sites) in Fig. 1(a) is two times larger, than that of the outer

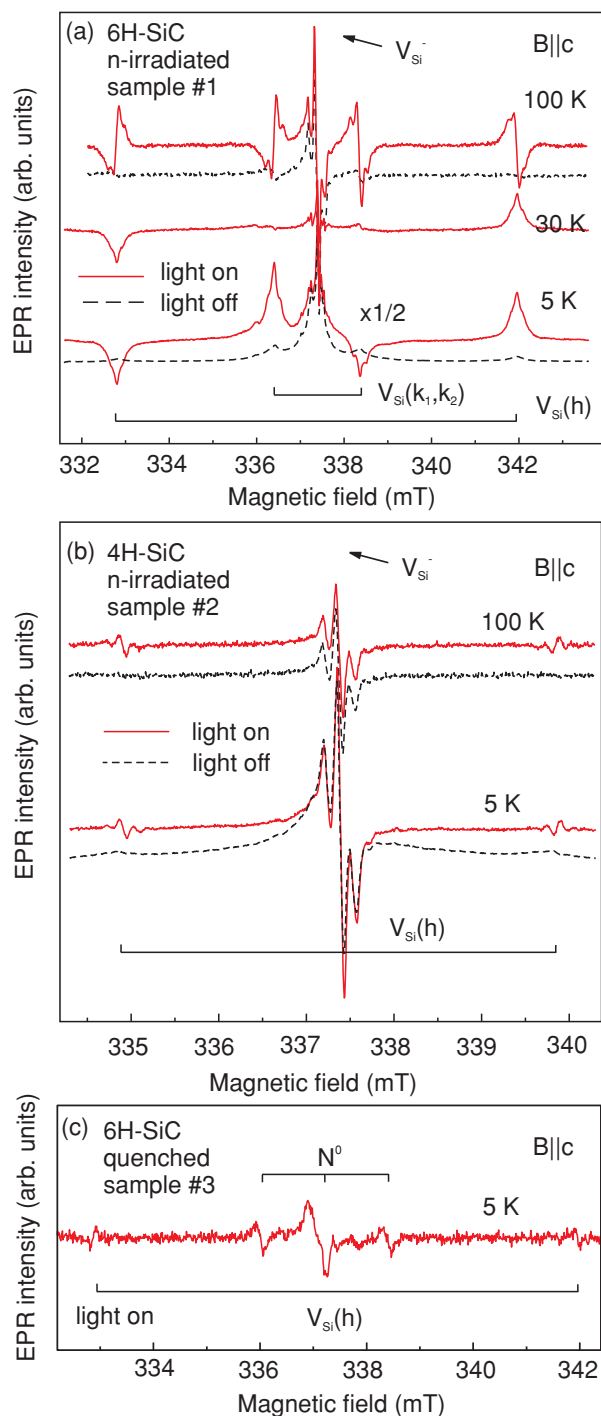


FIG. 1. (Color online) cw X-band (9.4 GHz) EPR spectra of Si vacancies detected under continuous optical illumination (solid line) and without optical illumination (dashed lines) with the magnetic field parallel to the  $c$  axis ( $B\parallel c$ ). (a) sample no. 1, (b) sample no. 2, (c) sample no. 3. Vertical bars indicate the positions of the lines for the  $V_{\text{Si}}$  in the hexagonal ( $h$ ) and quasicubic ( $k_1, k_2$ ) sites. The oblique solid arrow indicates the position of the central line of the  $V_{\text{Si}}^-$  vacancy. Additional lines belonging to nitrogen donors are shown in (c).

doublet ( $h$  site). A deviation from the first derivative of the EPR signal observed in Fig. 1(a) at low temperature is caused by saturation of the signal.

To date two possible models are proposed for the observed  $V_{\text{Si}}$  vacancy: neutral silicon vacancy  $V_{\text{Si}}^0$  with  $S = 1$ <sup>26–34</sup> and recently revised a low-symmetry modification of the well-studied negatively charged silicon vacancy  $V_{\text{Si}}^-$  in the regular environment<sup>25</sup> with  $S = 3/2$ .<sup>35–37</sup> In our opinion, in Ref. 35, sufficiently convincing arguments in favor of the revision of the model were not provided. First, the absence of zero-phonon lines for the classical vacancies  $V_{\text{Si}}^-$  was not explained as well as the difference between the electronic structure of two  $V_{\text{Si}}^-$  centers. Secondly, the ESE and ENDOR studies of the authors of Ref. 35 cannot be unambiguously interpreted because the observed ESE and ENDOR signals may be a superposition of the signal of the classical  $V_{\text{Si}}^-$  vacancy with  $S = 3/2$  whose intensity is several orders of magnitude higher, than those of the  $V_{\text{Si}}^0$  vacancy. Thirdly in electron-nuclear double-resonance experiments presented the nature of some intense lines has not been explained and, for an unclear reason, the measurements have been performed only at room temperature and with only one type of vacancy. We cannot, however, exclude this model from the discussion and will deal fairly with both  $V_{\text{Si}}^0$  ( $S = 1$ ) and  $V_{\text{Si}}^-$  ( $S = 3/2$ ) even though we support the former.

It is evident from Fig. 1 that under optical pumping the intensity of the EPR spectra grows substantially and a phase reversal is observed for one of the two transitions in each pair of lines. For instance, for the  $k_1$  and  $k_2$  positions in 6H-SiC at low temperatures (below 30 K) and for the  $h$  positions in 4H-SiC at all temperatures, a phase reversal is observed for the high-field transition, while for the  $k_1$  and  $k_2$  positions in 6H-SiC at high temperatures (above 30 K) and for the  $h$  positions in 6H-SiC at all temperatures a phase reversal is observed for the low-field transition. As a result of the optical pumping, the distribution of the populations of the spin sublevels in the ground state departs from a Boltzmann distribution. Even an inverse population is created between certain spin sublevels, and emission rather than absorption is detected for one of the transitions (high-field or low-field, depending on the polytype, crystal position, and temperature). The enhancement of the EPR signal under optical excitation has led in the past to the suggestion that the EPR spectra of such systems (NV defect in diamond, neutral Si vacancy, and Si-C divacancy in SiC) belong to excited states. Based on a study of the EPR spectra of the neutral silicon vacancies<sup>31,32</sup> and a C-Si divacancy<sup>38</sup> at 95 GHz and low temperatures (1.2–1.5 K) in full darkness, it was unambiguously shown that these spectra belonged to the high-spin ground state and that the sign of the fine-structure splitting  $D$  is positive. At a temperature of 30 K and with optical excitation the signal for the  $k_1$  and  $k_2$  positions in 6H-SiC disappears indicating that at this temperature the spin-lattice relaxation rates destroy the optical alignment.

Considering that the EPR spectra shown in Fig. 1 related to the neutral silicon vacancy  $V_{\text{Si}}^0$  with  $S = 1$  two possible energy levels schemes of the triplet sublevels for the ground state of the vacancy in a magnetic field under optical alignment are proposed in Figs. 2(a) and 2(b). In Fig. 2(a) the  $M_S = 0$  level is predominantly populated upon optical pumping whereas in the Fig. 2(b) scheme the  $M_S = \pm 1$  levels are predominantly populated. The populations of the sublevels are indicated by different numbers of filled circles. In Figs. 2(c) and 2(d), the optical alignment process of the triplet sublevels of the ground state in zero magnetic field of the neutral  $V_{\text{Si}}$  vacancy

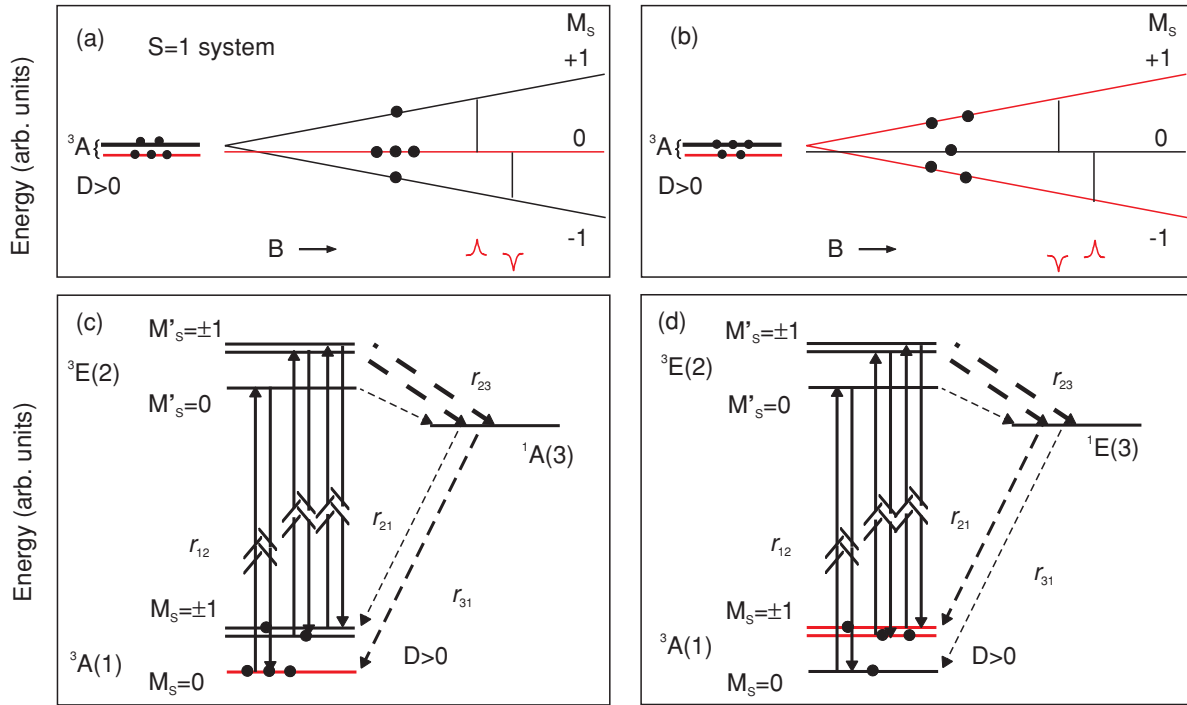


FIG. 2. (Color online) (a),(b) Two energy-level schemes for opposite types of optical alignment of the spin sublevels for the ground state of the Si vacancy in magnetic field on the assumption of the  $V_{\text{Si}}^0$  with  $S = 1$  model. (a)  $M_S = 0$  level is predominantly populated upon optical pumping, thus the high magnetic-field transition is emissive, (b)  $M_S = \pm 1$  levels are predominantly populated and the low magnetic-field transition is emissive. The populations of the ground-state energy levels under optical pumping are indicated by different numbers of filled circles. (c) and (d) Seven-level models interpreting the optical alignment of the ground-state sublevels in zero magnetic field for two schemes. Solid and dashed lines indicate the radiative and nonradiative transitions, respectively. The oblique dashed thick arrow indicates the most probable ISC transition, double line of the upper sublevels for the  ${}^3A$  and  ${}^3E$  states indicates that these levels are doubly degenerate. For the  ${}^3E$  state only the lower three levels are indicated.

is presented for the two possible energy levels schemes shown. The scheme comprises the  ${}^3A$  ground state, the  ${}^3E$  excited state, and a metastable singlet state. For the  ${}^3E$  state only the lower three levels are indicated. Luminescence and optical absorption correspond to transitions between the sublevels of the  ${}^3E$  and  ${}^3A$  states.

To explain the photokinetic processes leading to spin alignment under optical pumping, the presence of the excited metastable singlet state is suggested and a spin-dependent intersystem crossing (ISC) between the  ${}^3E$  state, the metastable singlet state and the  ${}^3A$  ground state. The vertical solid arrows and the oblique dashed arrows indicate the radiative and nonradiative transitions, respectively. The  ${}^3A$ - ${}^3E$  transition is orbitally allowed and the optical cycling of the  ${}^3A$ - ${}^3E$  transition will not result in a change of spin state and will not lead to a spin alignment. However, spin alignment can result from ISC from the  ${}^3E$  state to the metastable singlet state (states) followed by decay to the  ${}^3A$  ground state. It is known that spin-orbit interaction mixes singlet and triplet states which transform according to the same irreducible representation. Assuming that the optical induced spin polarization is faster than the spin-lattice relaxation, theoretically the spin polarization could be up to 100%.

As a working model for the  $V_{\text{Si}}^0$  ( $S = 1$ ) vacancy that is consistent with the scheme in Figs. 2(a) and 2(c) we will utilize the model developed for the NV defect in diamond in Refs. 39–42. Here the radiative lifetime of 13 ns (close

in magnitude to that for Si vacancy in SiC) corresponds to a decay rate of  $77 \times 10^6 \text{ s}^{-1}$ .<sup>39–41</sup> In this model it was assumed that there are two components in the emission decay, one associated with the sublevels  $M'_S = 0$  and one with  $M'_S = 1$ . It was suggested that the rate  $r_{23}$  of the transition from the  $M'_S = 1$  sublevels of the excited  ${}^3E$  state (2) to the metastable singlet  ${}^1A$  state (3) [oblique thick dashed arrow in Fig. 2(c)] is much larger than the rates of the transition from the  $M'_S = 0$  sublevel. Further the rates of the transitions  $r_{31}$  between  ${}^1A$  (3) and the sublevel  $M_S = 0$  of the  ${}^3A$  ground state (1) [the oblique thick dashed arrow in Fig. 2(c)] is much larger than the rates of the transitions from  ${}^1A$  to  $M_S = 1$  of the ground state. As a result, the spin sublevel  $M_S = 0$  of the  ${}^3A$  ground state is predominantly populated and an inverse population is created. This scheme is realized for the  $k1$  and  $k2$  positions in 6H-SiC at low temperatures (below 30 K), for the  $h$  positions in 4H-SiC at all temperatures as observed in the EPR spectra, for the NV defect in diamond<sup>39–41</sup> and for the C-Si divacancy.<sup>38</sup>

In the second type of the optical alignment, corresponding to Figs. 2(b) and 2(d) the rate  $r_{23}$  of the transition from the  $M'_S = \pm 1$  sublevels of the excited  ${}^3E$  state (2) to the metastable singlet  ${}^1E$  state (3) [oblique thick dashed arrow in Fig. 2(d)] is again much larger than the rates of the transitions from the  $M'_S = 0$  sublevel, the rates of the transitions  $r_{31}$  between the singlet state  ${}^1E$  (3) and sublevel  $M_S = 0$  of the  ${}^3A$  ground state (1) [oblique thick dashed arrow in Fig. 2(c)] is much less however than the rates of the transitions from  ${}^1E$  to the levels

$M_S = \pm 1$  of the ground  $^3A$  state (1). As a result, the sublevels with  $M_S = \pm 1$  of the  $^3A$  ground state are predominantly populated [Figs. 2(b) and 2(d)]. This scheme is realized for the  $k1$  and  $k2$  positions in 6H-SiC at high temperatures (above 30 K) and for the  $h$  positions in 6H-SiC at all temperatures.

To our knowledge a theoretical model of the optical alignment for the  $S = 3/2$  system (case of  $V_{Si}^-$ ) has not been developed yet. However, considering that the same mechanisms are governing the optical alignment of the spin sublevels, one can suggest the similar models for the  $S = 3/2$  as those previously discussed. Under optical illumination either  $M_S = \pm 1/2$  or  $M_S = \pm 3/2$  are predominately populated [Figs. 3(a) and 3(b), respectively] and the reversal phase is observable for the low-field or high-field transitions, respectively. The population of the ground-state sublevels can deviate from a Boltzmann distribution under optical pumping due to the differences of the recombination rates of the transitions from the excited state to the ground state via metastable doublet state.

In the first type the rate  $r_{23}$  of the transition from the  $M_S = \pm 3/2$  sublevels of the excited  $^4E$  state (2) to the metastable doublet  $^2A$  state (3) [oblique thick dashed arrow in Fig. 3(c)] is much larger than the rates of the transition from the  $M_S = \pm 1/2$  sublevels. Further the rates of the transitions  $r_{31}$  between  $^2A$  (3) and the sublevels  $M_S = \pm 1/2$  of the  $^4A$  ground state (1) [oblique thick dashed arrow in Fig. 3(c)] is much larger than the rates of the transitions from  $^2A$  (3) to  $M_S = \pm 3/2$ .

As a result, the spin sublevels  $M_S = \pm 1/2$  in the  $^4A$  ground state is predominantly populated and an inverse population is created. Similar to the case of  $V_{Si}^0$  this scheme is realized for the  $k1$  and  $k2$  positions in 6H-SiC at low temperatures (below 30 K), for the  $h$  positions in 4H-SiC at all temperatures as observed in the EPR spectra.

In the second type, notwithstanding that the  $r_{23}$  rate of the transition from the  $M_S = \pm 3/2$  sublevels of the excited  $^4E$  state to the metastable doublet  $^2E$  is much larger than those from  $M_S = \pm 1/2$ , the rate  $r_{31}$  of the transition from the doublet  $^2E$  to the  $M_S = \pm 3/2$  of the  $^4A$  is much larger than to the  $M_S = \pm 1/2$  [see oblique thick lines in Fig. 3(d)].

The observed change in the optical alignment of the ground-state spin sublevels of the silicon vacancy with temperature increase indicates that electron-phonon interactions lead to a significant change in the character of spin-dependent recombination upon excitation with unpolarized light. The absence of an EPR signal for the  $k1$  and  $k2$  positions in 6H-SiC at 30 K (and for the  $k$  position in 4H-SiC in the entire temperature range) indicates that all the spin sublevels of the ground state seem to be equally populated. It follows from our experiments that the local crystal field at the vacancy position also exerts a determining effect on the optical alignment scheme, leading to a difference in the splitting of the sublevels in the excited state and, as a consequence, to a difference in the probabilities of intersystem transitions between the  $^3E$  and the metastable singlet states.

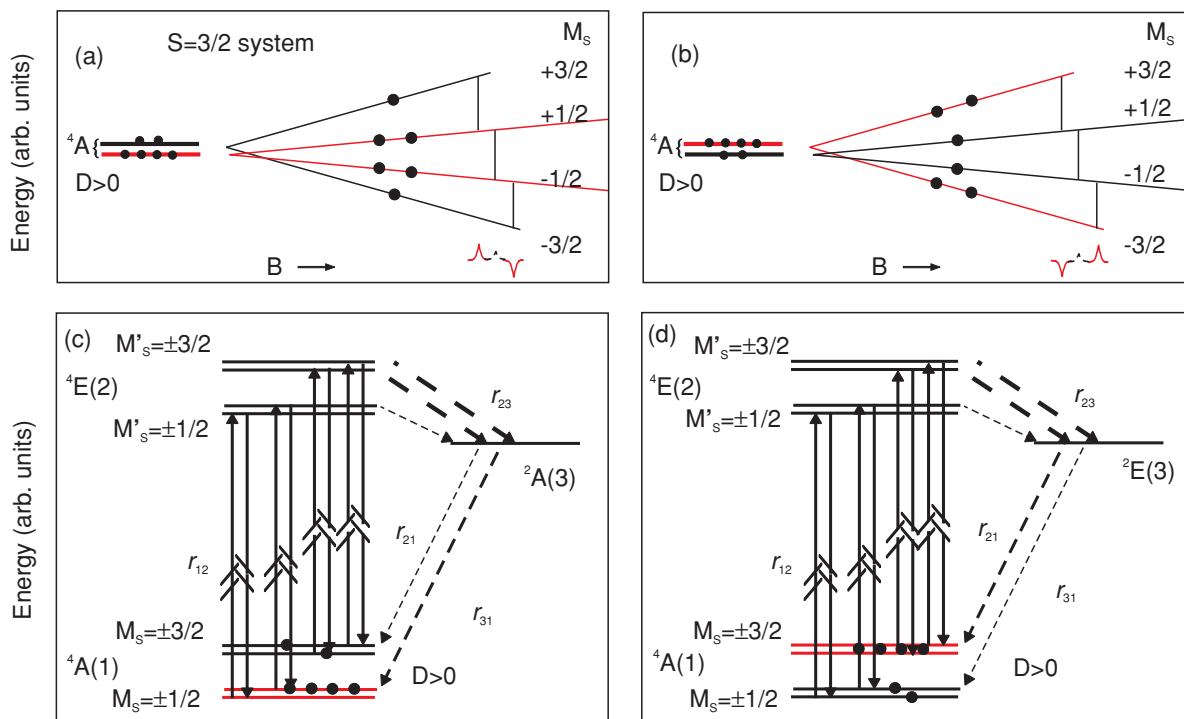


FIG. 3. (Color online) (a),(b) Two energy-level schemes for opposite types of optical alignment of the spin sublevels for the ground state of the Si vacancy in magnetic field on the assumption of the  $V_{Si}^-$  with the  $S = 3/2$  model. (a)  $M_S = \pm 1/2$  level is predominantly populated upon optical pumping, thus the high magnetic-field transition is emissive; (b)  $M_S = \pm 3/2$  levels are predominantly populated and the low magnetic-field transition is emissive. The populations of the ground-state energy levels under optical pumping are indicated by different numbers of filled circles. (c) and (d) Nine-level models interpreting the optical alignment of the ground-state sublevels in zero magnetic field for two schemes. Solid and dashed lines indicate the radiative and nonradiative transitions, respectively. The oblique dashed thick arrow indicates the most probable ISC transition. For the  $^4E$  state only the lower four levels are indicated.

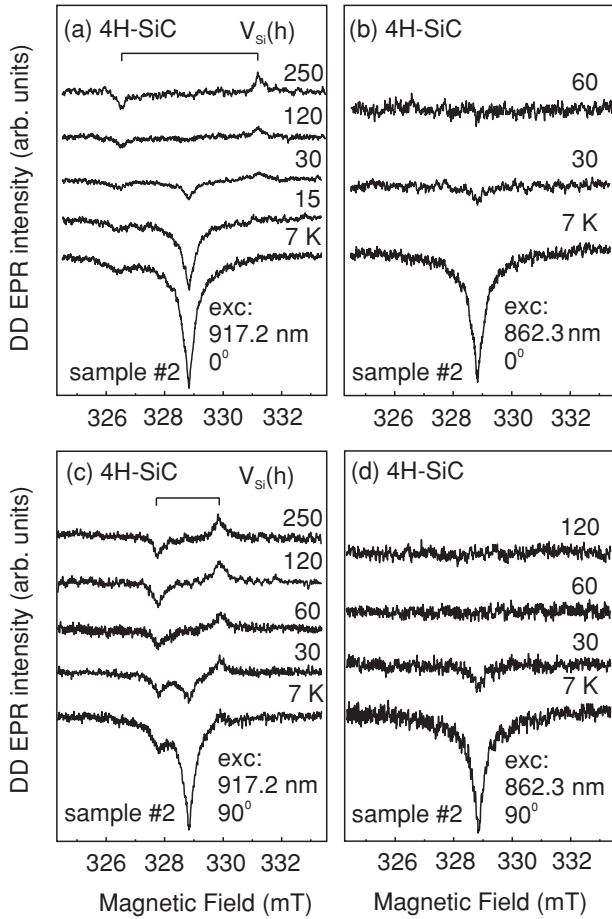


FIG. 4. The light-induced signals in the 4H-SiC single crystal (sample no. 2) detected at different temperatures by the DD-EPR technique with the magnetic field parallel  $\theta = 0^\circ$  (a),(b) and perpendicular  $\theta = 90^\circ$  (c),(d) to the  $c$  axis. The sample is selectively excited into the absorption band of the ZPLs attributed to the hexagonal  $h$  site at 917.2 nm (a),(c) and to the quasicubic  $k$  site at 862.3 nm (b),(d). Vertical bars indicate the positions of the lines for the  $V_{\text{Si}}$  vacancy in the  $h$  site for two orientations.

### B. Direct-detection EPR

Figure 4 shows the light-induced EPR signals obtained with the direct-detection EPR technique of the silicon vacancies in a 4H-SiC single crystal (sample no. 2) for two orientations:  $0^\circ$  ( $B \parallel c$ ) (a),(b) and  $90^\circ$  ( $B \perp c$ ) (c),(d) these silicon vacancies  $V_{\text{Si}}$  were selectively excited into their zero-phonon absorption bands at 917.2 nm (a),(c) and 862.3 nm (b),(d) at different temperatures by a pulsed laser with a pulse duration of 20 ns. A boxcar gate of 4–5  $\mu\text{s}$  at a delay after the flash of 0.5 or 1  $\mu\text{s}$  detects the spectra. The vertical bars indicate the positions of the lines for the  $V_{\text{Si}}$  vacancy in the hexagonal ( $h$ ) site for two orientations. EPR and ODMR signals could be attributed to the two different vacancy positions  $h$  and  $k$ . In Fig. 4 only the  $h$  position is presented.

The central line present in all DD-EPR spectra in Fig. 4 seems to belong to the negatively charged Si vacancy which is temporarily induced by the optical excitation in consideration that the charge state of the silicon vacancy is neutral. A similar effect was observed in Ref. 43 for vacancies in alkali halide crystals. An electron was discovered to tunnel from the relaxed

excited state of the F center in KCl (neutral vacancy) under optical excitation into the absorption band of the F center to a nearby F center, forming an intermediate F center (negatively charged vacancy). From this negatively charged vacancy it can tunnel back into the ground state of the original F-center site. In this mechanism it is essential that an F center can temporarily trap a second electron and form an F center. Thus here we can also consider a mechanism for the electron (charge) transfer (tunneling) from the excited state of a  $V_{\text{Si}}^0$  to a nearby  $V_{\text{Si}}^0$  forming an intermediate center in the form of  $V_{\text{Si}}^-$ . From this  $V_{\text{Si}}^-$  the electron can tunnel back into the ground state of the original  $V_{\text{Si}}^0$ .

Under optical pumping, a phase reversal is observed for the high-field transition of  $V_{\text{Si}}(h)$  in 4H-SiC at all temperatures [Figs. 4(a) and 4(c)]. As a result of the optical alignment the distribution of the populations of the spin sublevels in the ground state departs from a Boltzmann distribution, an inverse population is created between certain spin sublevels, and emission rather than absorption is detected for the high-field transitions. Apparently the first optical alignment scheme presented in Fig. 2(a) [Fig. 3(a)] applies to  $V_{\text{Si}}(h)$  in 4H-SiC at all temperatures. As a result of the optical illumination into the ZPL of 917.2 nm in 4H-SiC, the spin sublevel with  $M_S = 0$  ( $M_S = \pm 1/2$ ) in the  $^3A$  ( $^4A$ ) ground state is predominantly populated and an inverse population is created.

The intensity of the DD-EPR signal depends on the excitation wavelength because even at high temperatures the ZPLs are still narrow (about 5 nm). The temperature behavior of the signals at two different wavelength of excitation is different. It is visible that the central line is temperature dependent and almost not detectable at 30 K. The relaxation seems to become too fast or the lifetime of the signals at the two wavelengths of the excitation become too short to be detected even at high time resolution. The intensity of the outer lines (left figure) for  $B \perp c$  is almost independent of temperature. A remarkable result from Fig. 4(a) is that the signal for  $B \parallel c$  becomes even more intense and sharper when the temperature is rising. These results additionally confirm that the spin alignment due to the optical pumping occurred in the neutron-irradiated samples and that the optical alignment can be observed at least up to 250 K. Moreover, the reduction of the intensity of the EPR lines with the temperature increase was not observed allowing one to expect that the alignment can be observed up to the room temperature.

### C. High-resolution fluorescence-excitation spectroscopy and zero-field ODMR

The photoluminescence (PL) (or fluorescence) spectra of Si vacancies in SiC represent a series of ZPLs whose number agrees in general with the number of inequivalent lattice sites in the SiC polytype. In 6H-SiC these lines arise at wavelengths of 865 nm ( $V_1$ ), 887 nm ( $V_2$ ), and 906 nm ( $V_3$ ) and for 4H-SiC at 862 nm ( $V_1$ ) and 917 nm ( $V_2$ ).

Thus, two and three ZPLs are observed in the 4H-SiC and 6H-SiC polytypes, respectively, accompanied by phonon replicas. PL spectra recorded in 6H-SiC single crystal irradiated by fast neutrons (sample no. 1) at 77 K (top) and at room temperature (bottom) under excitation with light of commercial solid-state 405-nm laser are shown in

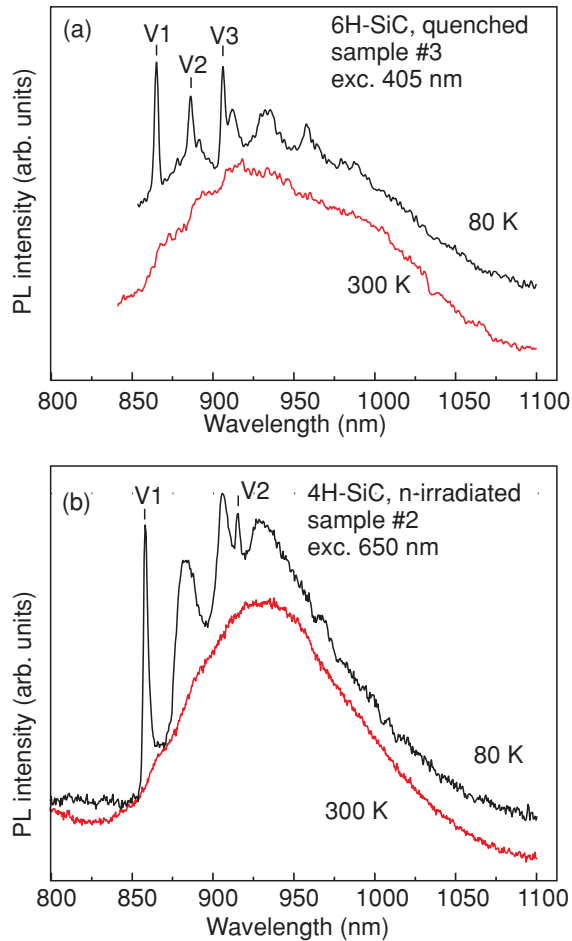


FIG. 5. (Color online) (a) PL spectra recorded in neutron-irradiated 6H-SiC (sample no. 1) at 77 K and room temperature with excitation at 405 nm. (b) PL spectra recorded in neutron-irradiated 4H-SiC (sample no. 2) at 77 K and room temperature with excitation at 650 nm.

Fig. 5(a). Figure 5(b) depicts PL spectra under excitation on the wavelength of 650 nm in neutron irradiated 4H-SiC single crystal (sample no. 2) at 77 K (top) and at room temperature (bottom).

EPR spectra of Si vacancies were detected by monitoring the ZPLs in 6H-SiC polytype at 1.433 eV (346.50 THz) for V1 line, 1.398 eV (338.04 THz) for V2 line, and 1.368 eV (330.78 THz) for V3 line and in 4H-SiC polytype at 1.438 eV (1.438 THz) for V1 line and 1.352 eV (1.352 THz) for V2 line and were first attributed to the neutral isolated Si vacancy ( $V_{Si}$ ) by the authors of Refs. 28 and 29. The assignment was based on the observed characteristic HF structure with the 12 Si atoms of the second shell that resembles the HF structure for the negatively charged isolated silicon vacancy  $V_{Si}^-$ . It is commonly accepted that the V1, V2, and V3 lines correspond to the  $k_1$ ,  $h$ , and  $k_2$  positions in 6H-SiC, respectively, and V1 and V2 lines correspond to the  $k$  and  $h$  sites in 4H-SiC, respectively.

A titanium-sapphire ring single-mode laser with a bandwidth of about 0.5 MHz was used to obtain high-resolution fluorescence-excitation spectra, by exciting the ZPLs attributed to the  $V_{Si}$  in the thermally as-quenched 6H-SiC

sample no. 3. The PL was detected at the peaks in the phonon-side-band part of the emission. The usual PL spectrum attributed to the Si vacancy in 6H-SiC with above-band-gap excitation consists of three narrow ZPLs between 860 and 910 nm indicated by V1, V2, and V3 and broad phonon replicas on the red side up to 1100 nm. Furthermore, an additional high-energy shoulder of V1 is detected in 6H-SiC, labeled V1\*, with a similar bandwidth to the three ZPLs.

High-resolution, fluorescence-excitation ZPLs of V1\*, V1, V3, and V2 are presented in Figs. 6(a), 6(b), 7(a), and 8(a) (curves 1 and 1'). All spectra contain only one absorption line. With an excitation intensity of 6.5 W/cm<sup>2</sup> absorption lines V1\* and V1 saturated and even at ten times lower excitation intensity the V1 line was still saturated. Figure 6(a) shows the high-resolution fluorescence-excitation spectra of the V1\* ZPL with single-mode laser excitation between 346.67 and 346.79 THz at 0.65 W/cm<sup>2</sup> (1) and 6.5 W/cm<sup>2</sup> (1'). The fluorescence-excitation spectra of V1 with single-mode laser excitation between 346.40 and 346.52 THz at 0.65 W/cm<sup>2</sup> is presented in Fig. 6(b), curve (1). The fluorescence-excitation spectrum of V3 saturated even at 0.1 W/cm<sup>2</sup>. Figure 7(a) shows the high-resolution fluorescence-excitation spectra of V3 with single-mode laser excitation between 330.72 and 330.85 THz at 1 W/cm<sup>2</sup> (1). No saturation of the V2 ZPL occurred with an excitation power up to 4.0 W/cm<sup>2</sup>. The high-resolution fluorescence-excitation spectra of V2 with single-mode laser excitation between 337.0 and 340.17 THz at 4 W/cm<sup>2</sup> (1) is shown in Fig. 8(a). The positions of the ZPLs and their inhomogeneous line widths are presented in Table I.

ODMR spectra were recorded in zero magnetic field with resonance excitation of the four zero-phonon bands, V1\*, V1, V2, and V3 in 6H-SiC. The experiments were carried out with a broad band (30 GHz) titanium-sapphire laser on thermally-quenched 6H-SiC single crystals (sample no. 3). The ODMR spectra obtained with excitation of the V1\* ZPL and detected at 937 nm is shown in Fig. 6(c). In addition a much weaker ODMR effect of opposite sign with an intensity of approximately 0.5% was observed at 130 MHz. This effect is visible in Fig. 6(c), curve (2), when the applied excitation energy was in the wing of the V1\* ZPL at 346.78 THz. A similar effect was observed for the V1 ZPL. The ODMR spectra obtained with excitation of the V3 ZPL detected at 958 nm is shown in Fig. 7(b). The spectra of V1 and V1\* consists of a broad feature from 10 to 60 MHz with three maxima at 16, 21, and 28 MHz and two weak shoulders at 40 and 52 MHz. The spectrum of V3, as visible in Fig. 7(b), is similar to the spectra of V1 and V1\*, i.e., a broad band up to 60 MHz with maxima at 16, 21 and 28 MHz and weak shoulders at 40 and 52 MHz.

Figure 8(b) shows the ODMR spectra obtained with excitation of the V2 ZPL and detection at 937 nm. The ODMR spectrum of V2 has its main feature at 130 MHz. Weaker satellites were observed at 24, 34, 44, and 66 MHz. The excitation energy corresponding to the maximum in the fluorescence-excitation spectrum yielded also the most intense ODMR effect. It should be noted that a small V2-like ODMR effect of opposite sign was observed when exciting around V1\* and V1 [Fig. 6(c)].

The ODMR effect on the intensity of the high-resolution fluorescence-excitation spectra obtained with a radio

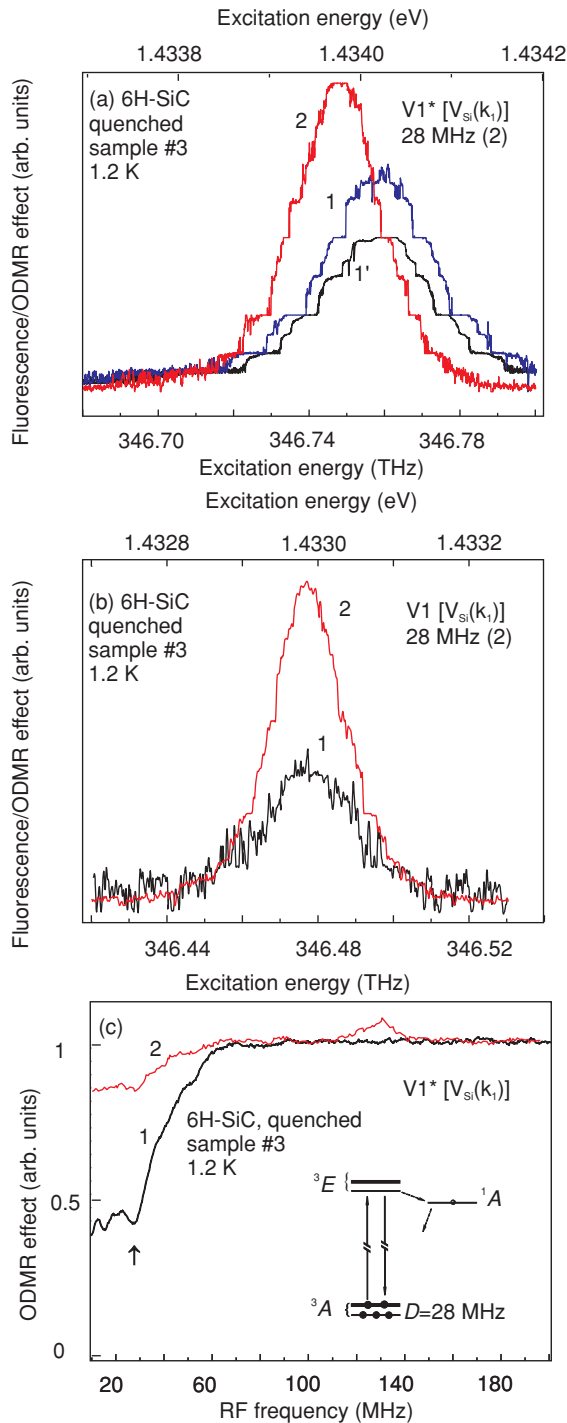


FIG. 6. (Color online) (a) High-resolution fluorescence-excitation spectra of  $V1^*$  with single-mode laser excitation between 346.67 and 346.79 THz at  $0.65 \text{ W/cm}^2$  (1) and  $6.5 \text{ W/cm}^2$  ( $1'$ ). Curve (2)—simultaneous excitation with a resonant rf field at 28 MHz. The optical excitation intensity is  $0.65 \text{ W/cm}^2$ . The spectra (1) and (2) are 10 times amplified. (b) The fluorescence-excitation spectra of  $V1$  with single-mode laser excitation between 345.40 and 346.52 THz at  $0.65 \text{ W/cm}^2$  (1). Curve (2)—ODMR excitation spectrum obtained with a resonant rf field at 28 MHz and the same laser power. (c) The ODMR spectra obtained with excitation of the  $V1^*$  ZPL with maximum ODMR effect detected at 937 nm. The small  $V2$ -like ODMR effect with the opposite sign is shown for an excitation at the wing of  $V1^*$  line at 346.78 THz.

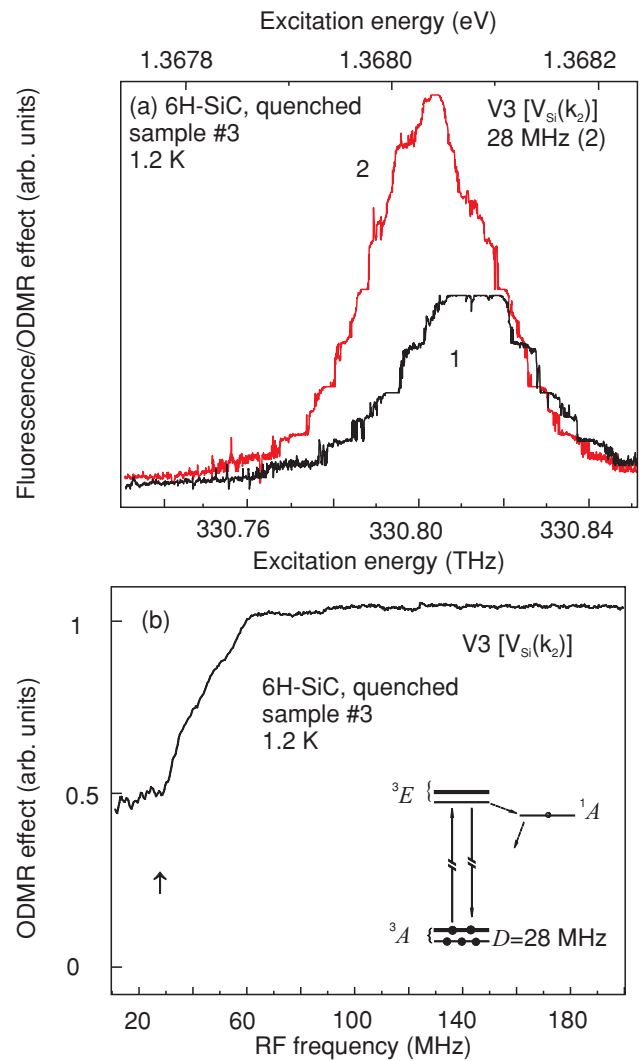


FIG. 7. (Color online) (a) The high-resolution fluorescence-excitation spectra of  $V3$  with single-mode laser excitation between 330.72 and 330.85 THz at  $1 \text{ W/cm}^2$  (1). Curve (2) is the ODMR excitation spectrum obtained with a resonant rf field at 28 MHz and the same laser power. (b) The ODMR spectra obtained with excitation of the  $V3$  ZPL with the maximum ODMR effect detected at 958 nm.

frequency of 28 MHz for the  $V1^*$ ,  $V1$ ,  $V3$  lines and 130 MHz for the  $V2$  line are presented in Figs. 6(a), 7(a), and 8(a), curves (2). For each line a strong ODMR effect is observed between 130 and 230% for different lines (see Table I). As one can see the ODMR excitation spectrum is shifted to lower energy (about 10 GHz) compared to that of the fluorescence-excitation spectrum for  $V1^*$ ,  $V1$ ,  $V3$  lines, and no shift of the maximum was observed for  $V2$  line. Thus, for  $V1^*$ ,  $V1$ , and  $V3$  the maximum ODMR effect appeared at lower excitation energy than the maximum in the fluorescence-excitation spectrum with the shift approximately 30 GHz. The large ODMR effect indicates the presence of a bottleneck state, which can be emptied by the resonance rf field. Thus, rf quanta of 28 and 130 MHz can efficiently control optical quanta in the range of 330–350 THz. For the  $V2$  line, saturation was not observed up to the available power of  $4 \text{ W/cm}^2$ , which makes this line the most promising for further detecting single defects.

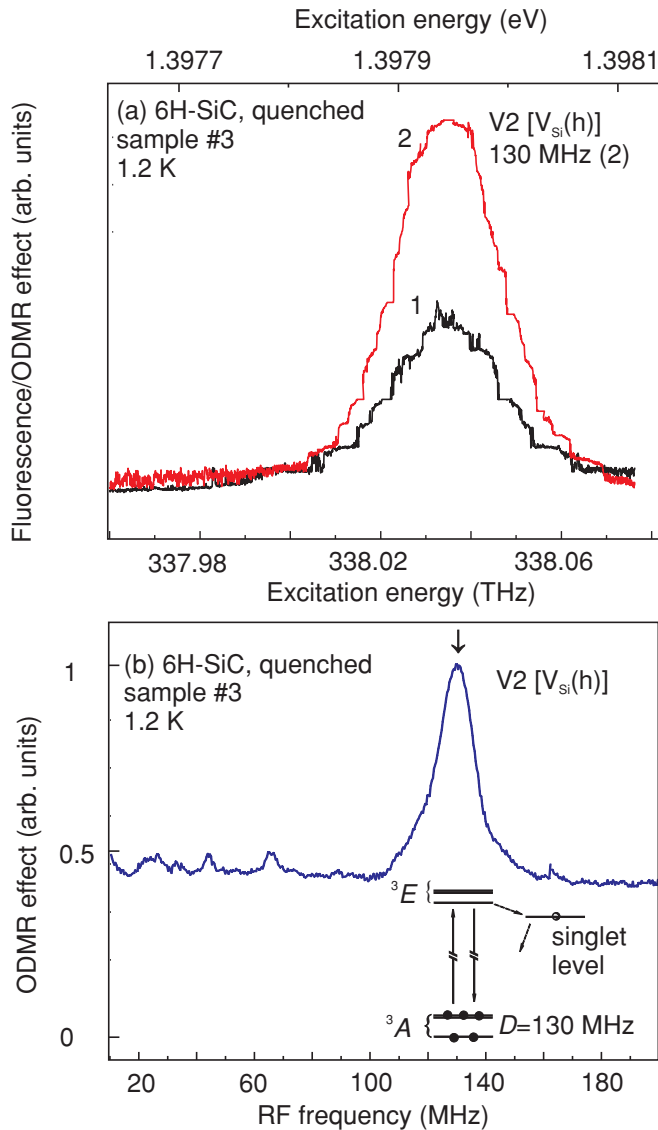


FIG. 8. (Color online) (a) The high-resolution fluorescence-excitation spectra of V2 with single-mode laser excitation between 337.95 and 341.07 THz at  $4 \text{ W/cm}^2$  (1). Curve (2) is the ODMR excitation spectrum obtained with a resonant rf field at 130 MHz and the same laser power. (b) The ODMR spectra obtained with excitation of the V3 ZPL with maximum ODMR effect detected at 937 nm.

#### D. The confocal arrangement for fluorescence-excitation spectroscopy and zero-field ODMR

To detect a small number of defects, even down to single defect, several conditions must be met. First, the excitation source must be at resonance with only one small group of defects (down to single defect) in the optical illuminated volume. Second, the PL from this small group of defects (single defect) should be larger than the background signal. To meet the first requirement confocal optics is used. To meet the second requirement, the PL should be detected in the phonon-side part of the ZPL to suppress excitation light. The  $V_{\text{Si}}$  has a broad phonon-side-band, which is well separated from the ZPLs, allowing this method of detection. Figure 9(a) shows the high-resolution fluorescence-excitation spectra at  $T = 1.4 \text{ K}$  in the thermally quenched 6H-SiC sample nos. 3, 3a, 3b, and 3c as detected at the phonon band using a confocal arrangement and a single-mode, tunable laser (bandwidth of 0.5 MHz): (a) around the V1 region; (b) around the V3 region. In Fig. 9(b) the high-resolution fluorescence-excitation spectra in neutron-irradiated sample no. 1 is also shown for comparison. For several lines their intensity (in counts per seconds) and linewidth (in MHz) are indicated. Surprisingly narrow ZPLs for Si vacancies with a width less than 0.05 meV are observed in Fig. 9. To our knowledge, the line widths observed in these experiments are the narrowest of those detected so far in SiC.

The high-resolution fluorescence experiments also indicate that the positions and the shape of the lines differ between the investigated samples apparently as a result of the annealing treatments. A short anneal at  $750^\circ\text{C}$  changes the structure of ZPLs considerably. Several groups of lines in the V1 and V3 regions appear. The different components of the V1 and V3 lines show a shift and the V2 line disappears after heating up to  $750^\circ\text{C}$ . This temperature of  $750^\circ\text{C}$  is the annealing temperature of the silicon vacancy in irradiated SiC.<sup>29</sup> Sequential annealing of the silicon vacancies was performed in order to reduce their amount and allowing the detection of the small groups of centers up to the single vacancy. As shown in Fig. 9 annealing lead to the appearance of several groups of lines with different intensity and width. The narrowness of the lines observed evidences the small concentrations of the Si vacancies. It is known that annealing induces a migration of the silicon vacancies through the SiC lattice. As a result the vacancy can be captured by extended defect structures, like, e.g., stacking faults (SF) or

TABLE I. The positions of the ZPLs in the emission and excitation spectra, inhomogeneous linewidth related to different sites of  $V_{\text{Si}}^0$  in 6H-SiC.

Site and line	Emission (eV)	Excitation (eV)	Linewidth (GHz)	Peaks of zero-field ODMR (MHz)	ODMR effect (%)
$k1$ (V1)	1.433	1.433 06	25	<b>28</b> 16,21,40,52	150
$k1$ (V1*)	1.434	1.434 22	30	<b>28</b> 16,21,40,52	130
$k2$ (V3)	1.368	1.368 28	30	<b>28</b> 16,21,40,52	130
$h$ (V2)	1.398	1.398 815	25	<b>128</b> 24,34,44,66	230

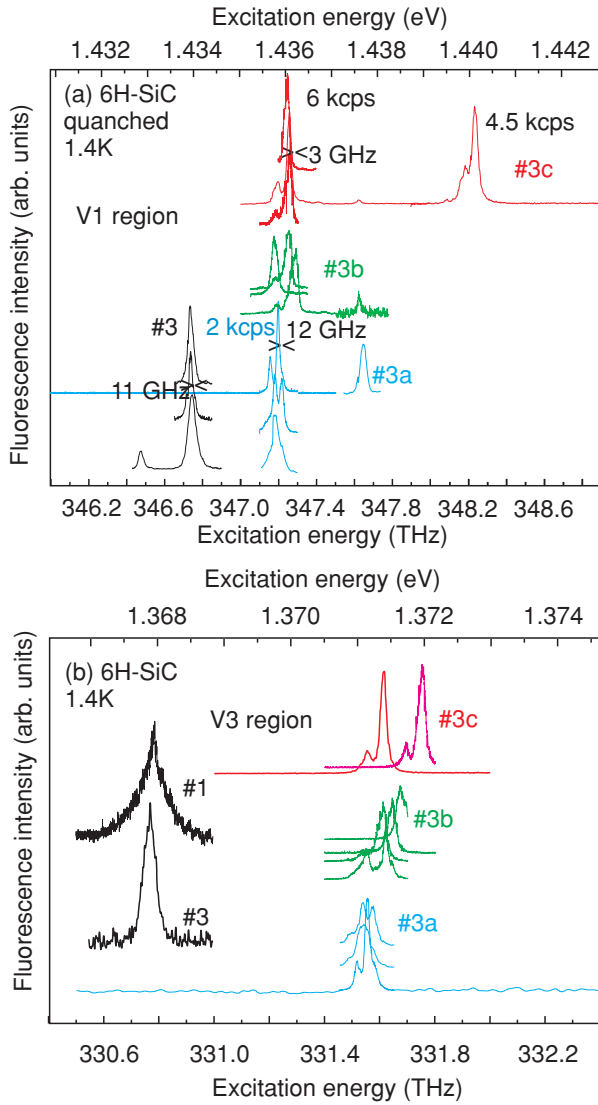


FIG. 9. (Color online) High-resolution fluorescence-excitation spectra around the V1 region (a) and around the V3 region (b) in the thermally quenched 6H-SiC sample nos. 3, 3a, 3b, and 3c and in neutron irradiated 6H-SiC sample no. 1. The detection is at the phonon band using a confocal arrangement and a single-mode tunable laser with a bandwidth of approximately 0.5 MHz. For all samples three spectra of the same color are shown recorded in the three different regions of the crystals. For several lines their intensity and linewidth indicated.

dislocations. One of the problems that need to be investigated and understood in order to fully develop SiC-based technology is the occurrence of SF.<sup>44</sup> Due to the small SF energy compared to other semiconductors such as Si or GaAs it is relatively easy to develop extended SF regions in SiC crystals, which, if electrically active, can seriously affect the device performance. SF, unlike point defects and surfaces, are not associated with broken or chemically perturbed bonds. Vacancies seem to tend to be attracted to a SF region due to strains.

The limit of the spatial resolution in the confocal experiments is about  $1 \mu\text{m}^3$  and is a factor 100 larger than the defect spacing needed for entanglement. To address chosen pairs

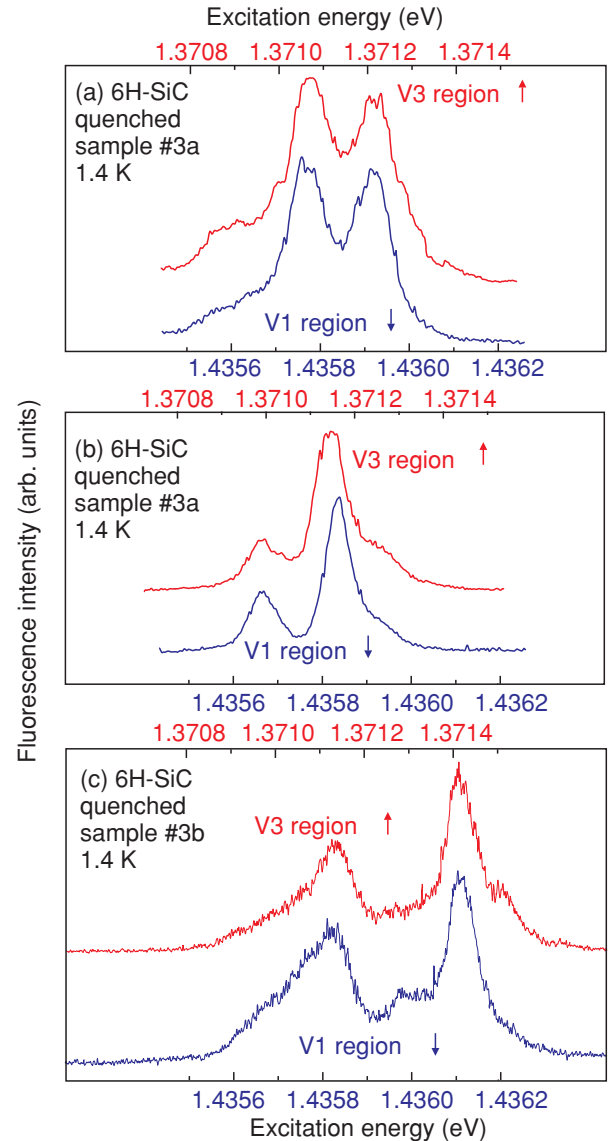


FIG. 10. (Color online) (a),(b) High-resolution fluorescence-excitation spectra are presented around the V1 region (bottom) and around the V3 region (top) in the thermally quenched and annealed 6H-SiC sample no. 3a. The spectra are measured at different positions in the sample. The single-mode laser, with a bandwidth of 0.5 MHz, excites the sample in the confocal arrangement and the detection takes place at phonon replicas. The scales correspond to the V1 region (bottom) and the V3 region (top). (c) Similar spectra obtained on sample no. 3b.

of qubits one can exploit the randomness of the interdefect distance in standard fabrication and doping.<sup>12</sup> Light at different wavelengths excites different defect spins in the confocal volume, as can be seen in Fig. 9, allowing manipulation of the entanglement of different qubits. Another attraction of the silicon vacancies in SiC is that the ZPLs occur in the range 850–920 nm, coinciding with the spectral window of silica glass optical fibers.

Figure 10 shows, on an extended-scale, the high-resolution fluorescence-excitation spectra around the V1 region (top) and around the V3 region (bottom) in the thermally quenched and annealed 6H-SiC sample nos. 3a (a),(b) and 3b (c). The spectra

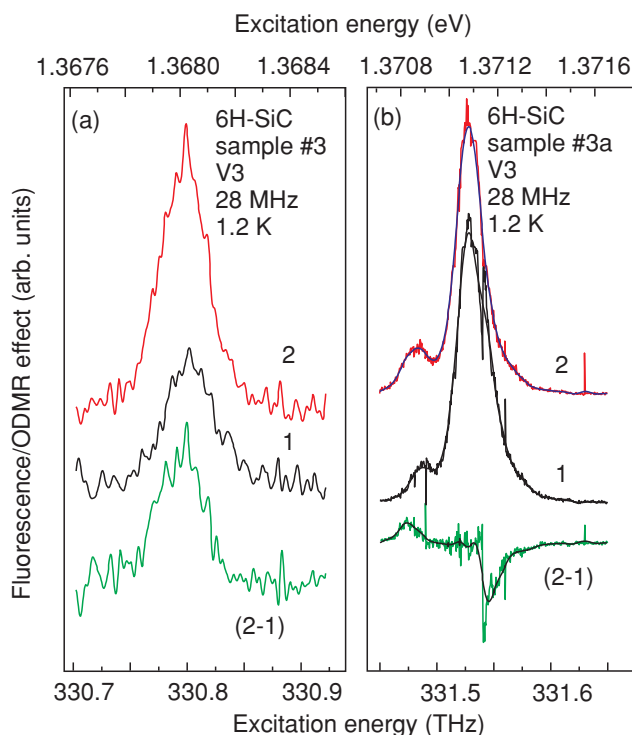


FIG. 11. (Color online) (a) The high-resolution, fluorescence-excitation spectra of the  $V3$  ZPL in the thermally quenched 6H-SiC sample no. 3. The single-mode laser excites the sample in the confocal arrangement and the detection is at the phonon band (1). The ODMR excitation spectrum obtained in the presence of a resonant rf field at 28 MHz at the same laser power (2) and the difference between the two spectra (2-1). (b) The high-resolution fluorescence-excitation spectra of the  $V3$  ZPL in the thermally quenched and annealed 6H-SiC sample no. 3a. The sample is excited with the single-mode tunable laser in the confocal arrangement with detection at the phonon band (1). Curve (2) is the ODMR excitation spectrum obtained in the presence of a resonant rf field at 28 MHz and the same laser power and the difference between two spectra (2-1).

are measured at different excitation points of the sample and are detected at phonon replicas using the confocal arrangement and excited by the single-mode tunable laser with a bandwidth of approximately 0.5 MHz. The upper scales correspond to the  $V1$  region (top) and the bottom scales to the  $V3$  region (bottom). A remarkable result is the correlation between the groups of ZPLs of the inequivalent quasicubic sites. These lines can be described as arising from quasicubic  $k1$  and  $k2$  positions of small groups of Si vacancies near some extended nonparamagnetic defects thus indicating the possibility of the optical pumping of the qubits states.

Figure 11 shows the high-resolution fluorescence-excitation spectra of the  $V3$  ZPL as detected at phonon side bands using again the confocal arrangement and excitation by the single-mode tunable laser (1). Spectrum (2) shows the excitation spectrum obtained with the simultaneous presence of a resonant radiofrequency field at 28 MHz. In Fig. 11(a) the results are shown on the thermally quenched 6H-SiC sample no. 3 and in Fig. 11(b) the results on the 6H-SiC sample no. 3a, thermally quenched and annealed at 750 °C. In the bottom of both figures the difference between the two spectra (2-1)

is plotted. Figure 11(a) shows that the excitation with resonant rf of 28 MHz, drastically affects the intensity of the luminescence. It is evident from a comparison of Figs. 8(a) and 11(a) that the spectra in the nonannealed sample measured with excitation of defects in a large spot of about 1 mm<sup>3</sup> [Fig. 8(a)] and in a small spot of about 1 μm<sup>3</sup> using the confocal arrangement [Fig. 11(a)], are similar. Another fluorescence-excitation pattern and an effect of rf excitation on the high-resolution fluorescence-excitation spectra of the  $V3$  ZPL have been observed in the thermally quenched and annealed sample [Fig. 11(b)]. Some lines are nearly unaffected by the rf of 28 MHz, that is, these lines seem to be characterized by different zero-field splittings. The decay time of the PL lines in 6H-SiC was shown in Ref. 29 to be about 8 ns for all three lines. The decay times stay constant at least from 2 to 70 K and the PL intensity does not change much in this temperature interval either. Our measurements show that ZPL can be observed up to room temperature.

The analogy between the properties of the Si vacancy ( $V_{Si}$ ) in SiC and the NV defect in diamond shows that the Si vacancy in SiC can be considered as a potential defect for quantum computing. The unique aspects of the silicon vacancy are: (i) the giant effect of resonant radiation on the intensity of ZPLs with a quantum yield close to unity; (ii) a convenient optical spectral range; (iii) the occurrence of several centers equivalent in their properties, which provides the possibility of selecting centers with the most attractive characteristics; (iv) the intrinsic nature of the defect; (v) the zero-field splitting of the silicon vacancy defect is much smaller than that for the NV defect in diamond and lies in the MHz range; (vi) the lifetime in the excited state is of the order of 10 ns, which is ideal for the detection of single defects; and (vii) the possibility to produce them by thermally treating the crystal without using ionizing irradiation; (viii) in contrast to the NV defects in diamond with four equivalent  $\langle 111 \rangle$  axis directions, all Si vacancies are characterized by the same axial symmetry along the  $c$  axis.

#### IV. CONCLUSION

EPR, zero-field ODMR, direct-detection EPR techniques, and high-resolution fluorescence-excitation spectroscopy using a confocal microscope and a single-mode laser were applied for the investigation of silicon vacancies in SiC single crystals. Two opposite schemes were observed for the optical alignment of the populations of the spin sublevels in the ground state of a Si vacancy in SiC upon illumination with unpolarized light. Optically induced inverse population of the spin sublevels in the zero magnetic field was observed for the first time, opening the possibility of obtainment of the maser effect on such systems. A change of a factor 2–3 was observed in the luminescence intensity of the zero-phonon lines in zero magnetic field upon absorption of radio waves with energy equal to the fine-structure splitting of spin sublevels of the vacancy ground state. This observation opens the possibility for magnetic-resonance detection of a single vacancy. As distinct from the known NV defect in diamond, the silicon vacancy is an intrinsic defect. In this system, the coherence time is expected to be longer than in the case of the NV defect, as the nitrogen atoms normally located in the diamond

lattice strongly influence the coherence time.<sup>9,10</sup> The electron spin of the Si vacancy can be manipulated by low-energy radio wave quanta in the range 20–150 MHz, which is two orders of magnitude lower than the corresponding energy for the NV defect in diamond. The optical alignment of the populations of spin sublevels in the ground state of a Si vacancy was shown with direct-detection EPR to be observable up to 250 K. Surprisingly narrow ZPLs for Si vacancies with a width less than 0.05 meV have been observed which seem to be the narrowest of those detected so far in SiC.

## ACKNOWLEDGMENTS

This work has been supported by the Ministry of Education and Science of the Russian Federation under Contracts No. 14.740.11.0048, 02.740.11.0108; the programs of RAS: “Spin-Dependent Effects in Solids and Spintronics”; “Support of Innovations and Elaborations”; “Basic Researches of Nanotechnologies and Nanomaterials,” and by the RFBR under Grants No. 09-02-01409 and 09-02-00730. We also would like to thank Daniel Tolmachev for photoluminescence measurements performed in 4H-SiC.

\*pavel.baranov@mail.ioffe.ru

†Present address: Eneco energy trade BV, P.O. Box 96, 2900 AB Capelle aan den IJssel, The Netherlands.

<sup>1</sup>T. Basche, W. E. Moerner, M. Orrit, and U. P. Wild, *Single-Molecule Optical Detection, Imaging and Spectroscopy* (VCH, Weinheim, 1997).

<sup>2</sup>J. Koehler, J. A. J. M. Disselhorst, M. C. J. M. Donckers, E. J. J. Groenen, J. Schmidt, and W. E. Moerner, *Nature (London)* **363**, 242 (1993).

<sup>3</sup>J. Wrachtrup, C. von Borczyskowski, J. Bernard, M. Orrit, and R. Brown, *Nature (London)* **363**, 244 (1993).

<sup>4</sup>J. Koehler, A. C. J. Brouwer, E. J. J. Groenen, and J. Schmidt, *Science* **268**, 1457 (1995).

<sup>5</sup>A. Gruber, A. Drabenstedt, C. Tietz, L. Fleury, J. Wrachtrup, and C. von Borczyskowski, *Science* **276**, 2012 (1997).

<sup>6</sup>F. Jelezko and J. Wrachtrup, *Phys. Status Solidi A* **203**, 3207 (2006).

<sup>7</sup>F. Jelezko, I. Popa, A. Gruber, C. Tietz, J. Wrachtrup, A. Nizovtsev, and S. Kilin, *Appl. Phys. Lett.* **81**, 2160 (2002).

<sup>8</sup>A. P. Nizovtsev, S. Ya. Kilin, F. Jelezko, I. Popa, A. Gruber, and J. Wrachtrup, *Physica B* **340–342**, 106 (2003).

<sup>9</sup>T. Gaebel, M. Domhan, I. Popa *et al.*, *Nature Physics* **2**, 408 (2006).

<sup>10</sup>T. A. Kennedy, J. S. Colton, J. E. Butler, R. C. Linares, and P. J. Doering, *Appl. Phys. Lett.* **83**, 4190 (2003).

<sup>11</sup>T. Gaebel, I. Popa, A. Grüber, M. Domhan, F. Jelezko, and J. Wrachtrup, *New J. Phys.* **6**, 98 (2004).

<sup>12</sup>M. Stoneham, *Physics* **2**, 34 (2009).

<sup>13</sup>M. V. Muzafarova, I. V. Ilyin, E. N. Mokhov, V. I. Sankin, and P. G. Baranov, *Mater. Sci. Forum* **527–529**, 555 (2006).

<sup>14</sup>J. R. Weber, W. F. Koehl, J. B. Varley, A. Janotti, B. B. Buckley, C. G. Van de Walle, and D. D. Awschalom, *Proc. Natl. Acad. Sci.* **107**, 8513 (2010).

<sup>15</sup>D. DiVincenzo, *Nat. Mater.* **9**, 468 (2010).

<sup>16</sup>P. G. Baranov, A. P. Bundakova, I. V. Borovykh, S. B. Orlinskii, R. Zondervan, and J. Schmidt, *JETP Lett.* **86**, 202 (2007).

<sup>17</sup>A. A. Lebedev, *Semiconductors* **33**, 107 (1999).

<sup>18</sup>Yu. A. Vodakov, E. N. Mokhov, G. Ramm *et al.*, *Krist. Techn.* **14**, 729 (1979).

<sup>19</sup>P. G. Baranov, B. Ya. Ber, O. N. Godisov *et al.*, *Phys. Solid State* **47**, 2219 (2005).

<sup>20</sup>P. G. Baranov, B. Ya. Ber, I. V. Ilyin *et al.*, *J. Appl. Phys.* **102**, 063713 (2007).

<sup>21</sup>G. Watkins, in *Deep Centers in Semiconductors*, edited by S. T. Pantelides (Gordon and Breach, New York, 1986), p. 147.

<sup>22</sup>M. K. Bosch, I. I. Proskuryakov, P. Gast, and A. J. Hoff, *J. Phys. Chem.* **100**, 2384 (1996).

<sup>23</sup>I. V. Borovykh, I. I. Proskuryakov, I. B. Klenina, P. Gast, and A. J. Hoff, *J. Phys. Chem. B* **104**, 4222 (2000).

<sup>24</sup>V. G. Grachev, *JETP* **65**, 1029 (1987).

<sup>25</sup>T. Wimbauer, B. K. Meyer, A. Hofstaetter, A. Scharmann, and H. Overhof, *Phys. Rev. B* **56**, 7384 (1997)

<sup>26</sup>V. S. Vainer and V. A. Il'in, *Sov. Phys. Solid State* **23**, 2126 (1981) [*Fiz. Tverd. Tela* **23**, 3659 (1981)].

<sup>27</sup>H. J. von Bardeleben, J. L. Cantin, I. Vickridge, and G. Battistig, *Phys. Rev. B* **62**, 10126 (2000).

<sup>28</sup>H. J. von Bardeleben, J. L. Cantin, L. Henry, and M. F. Barthe, *Phys. Rev. B* **62**, 10841 (2000).

<sup>29</sup>E. Sörman, N. T. Son, W. M. Chen, O. Kordina, C. Hallin, and E. Janzen, *Phys. Rev. B* **61**, 2613 (2000); E. Sörman, W. M. Chen, N. T. Son, C. Hallin, J. L. Lindström, B. Monemar, and E. Janzen, *Mater. Sci. Forum* **264–268**, 473 (1998).

<sup>30</sup>M. Wagner, B. Magnusson, W. M. Chen, E. Janzen, E. Sörman, C. Hallin, and J. L. Lindström, *Phys. Rev. B* **62**, 16555 (2000).

<sup>31</sup>P. G. Baranov, E. N. Mokhov, S. B. Orlinskii, and J. Schmidt, *Physica B* **308–310**, 680 (2001).

<sup>32</sup>S. B. Orlinski, J. Schmidt, E. N. Mokhov, and P. G. Baranov, *Phys. Rev. B* **67**, 125207 (2003).

<sup>33</sup>M. Wagner, N. Q. Thinh, N. T. Son, W. M. Chen, E. Janzen, P. G. Baranov, E. N. Mokhov, C. Hallin, and J. L. Lindström, *Phys. Rev. B* **66**, 155214 (2002).

<sup>34</sup>N. T. Son, Z. Zolnai, and E. Janzen, *Phys. Rev. B* **68**, 205211 (2003).

<sup>35</sup>N. Mizuochi, S. Yamasaki, H. Takizawa, N. Morishita, T. Ohshima, H. Itoh, and J. Isoya, *Phys. Rev. B* **66**, 235202 (2002); N. Mizuochi, S. Yamasaki, H. Takizawa, N. Morishita, T. Ohshima, H. Itoh, T. Umeda, and J. Isoya, *ibid.* **72**, 235208 (2005).

<sup>36</sup>E. Janzen, A. Gali, P. Carlsson *et al.*, *Physica B* **404**, 4354 (2009).

<sup>37</sup>N. T. Son, P. Carlsson, J. ul Hassan B. Magnusson, and E. Janzen, *Phys. Rev. B* **75**, 155204 (2007).

<sup>38</sup>P. G. Baranov, I. V. Il'in, E. N. Mokhov, M. V. Muzafarova, S. B. Orlinskii, and J. Schmidt, *JETP Lett.* **82**, 441 (2005).

<sup>39</sup>J. Harrison, M. J. Sellars, and N. B. Manson, *J. Lumin.* **107**, 245 (2004); *Diam. Relat. Mater.* **15**, 586 (2006).

<sup>40</sup>N. B. Manson, J. P. Harrison, and M. J. Sellars, *Phys. Rev. B* **74**, 104303 (2006).

<sup>41</sup>N. B. Manson and R. L. McMurtrie, *J. Lumin.* **127**, 98 (2007).

<sup>42</sup>V. M. Acosta, A. Jarmola, E. Bauch, and D. Budker, *Phys. Rev. B* **82**, 201202 (2010).

<sup>43</sup>F. Porret and F. Lüty, *Phys. Rev. Lett.* **26**, 843 (1971).

<sup>44</sup>H. Iwata, U. Lindefelt, S. Oberg, and P. R. Briddon, *Phys. Rev. B* **65**, 033203 (2001).